Chinese Physics B

PAPER

Effect of thickness variations of lithium niobate on insulator waveguide on the frequency spectrum of spontaneous parametric down-conversion*

To cite this article: Guang-Tai Xue *et al* 2021 *Chinese Phys. B* **30** 110313

Effect of thickness variations of lithium niobate on insulator waveguide on the frequency spectrum of spontaneous parametric down-conversion*

Guang-Tai Xue(薛广太)[1], Xiao-Hui Tian(田晓慧)[1], Chi Zhang(张弛)[1], Zhenda Xie(谢臻达)[1], Ping Xu(徐平)[2], Yan-Xiao Gong(龚彦晓)[1,†], and Shi-Ning Zhu(祝世宁)[1]

[1] *National Laboratory of Solid State Microstructures, School of Physics, School of Electronic Science and Engineering, College of Engineering and Applied Sciences, and Collaborative Innovation Center of Advanced Microstructures, Nanjing University, Nanjing* 210093, *China*

[2] *Institute for Quantum Information and State Key Laboratory of High Performance Computing, College of Computing, National University of Defense Technology, Changsha* 410073, *China*

(Received 17 August 2021; revised manuscript received 27 August 2021; accepted manuscript online 1 September 2021)

We study the effect of waveguide thickness variations on the frequency spectrum of spontaneous parametric down-conversion in the periodically-poled lithium niobate on insulator (LNOI) waveguide. We analyze several variation models and our simulation results show that thickness variations in several nanometers can induce distinct effects on the central peak of the spectrum, such as narrowing, broadening, and splitting. We also prove that the effects of positive and negative variations can be canceled and thus lead to a variation-robust feature and an ultra-broad bandwidth. Our study may promote the development of on-chip photon sources in the LNOI platform, as well as opens up a way to engineer photon frequency state.

Keywords: lithium niobate on insulator, spontaneous parametric down-conversion, waveguide thickness variation, frequency spectrum

PACS: 03.67.−a, 42.50.−p, 42.82.−m, 42.65.−k **DOI:** 10.1088/1674-1056/ac22a1

1. Introduction

Thin-film lithium niobate on insulator (LNOI)[1,2] is thought to be a revolutionary platform for integrated photonics,[3,4] since it allows strong optical confinement and a high integration density on lithium niobate (LN), a material possessing superior optical performance,[5] such as low optical transmission losses, large electro-optical and second-order nonlinear coefficients. In recent years, LNOI-based integrated photonic devices have achieved remarkable breakthroughs, such as low-loss waveguides,[6–9] high-quality-factor microring resonators,[7,10] high-speed electro-optic modulators,[11,12] and broadband optical frequency comb generation.[13,14]

Quasi-phase-matching (QPM)[15] spontaneous parametric down-conversion (SPDC) in periodically-poled crystals or waveguides,[16,17] typically periodically-poled LN (PPLN),[18–22] is widely used in the generation of entangled photon pairs, for the merits of high efficiency and frequency tunability. Benefiting from the strong optical confinement, ultrahigh-efficiency SPDC processes in periodically-poled LNOI (PPLNOI) waveguides were demonstrated recently.[23–25] In particular, a PPLNOI waveguide source with a brightness two orders of magnitude higher than that in the traditional PPLN waveguide was achieved in our lab,[25] as the cross-sectional area of the LNOI waveguide was ~ 2 orders of magnitude smaller than that of the traditional LN waveguide. However, in practical experiment the nonlinear optical performance may be affected by imperfections in fabrication of the waveguide.[26–28] With stronger light confinement, such effect in LNOI-based devices could become greater. Recently, Tian *et al.*[26] revealed that the spectrum profile and efficiency can be greatly affected by the LNOI waveguide cross-section dimension variations, especially the thickness variations. Hence, with regard to developing photonic quantum technologies in the LNOI platform, it is of practical importance to study the effect of LNOI waveguide fabrication imperfections on SPDC.

In this paper, we make a study on the effect of thickness variations of the LNOI waveguide on the frequency spectrum of SPDC. Our simulation results show that the central peak of SPDC frequency spectrum can be greatly affected by the waveguide thickness variations. Our study can not only give a benchmark to the LNOI waveguide fabrication, but also provide a way for the manipulation of photon frequency state.

2. Basic principles and methods

We consider a PPLNOI waveguide with the schematic structure shown in Fig. 1(a). The LNOI wafer consists of three

*Project supported by the National Key R&D Program of China (Grant No. 2019YFA0705000), Leading-edge Technology Program of Jiangsu Natural Science Foundation, China (Grant No. BK20192001), and the National Natural Science Foundation of China (Grant Nos. 51890861, 11690031, 11974178, and 11627810).

†Corresponding author. E-mail: gongyanxiao@nju.edu.cn

layers from up to bottom. The top X-cut LN film with a thickness of $H = 600$ nm is etched to a depth of $h = 350$ nm with a bottom ridge width of $w = 1400$ nm and a sidewall angle of $\theta = 60°$. The middle is a 2-μm-thick silicon dioxide bonding layer and the bottom is a 0.5-mm-thick LN or silicon (Si) substrate. The length of the waveguide is L and the whole waveguide is poled with a period of Λ. Here we consider a type-0 QPM SPDC process converting the pump photons at 780 nm to frequency-degenerate photon pairs at 1560 nm. With the COMSOL software we simulate the field distributions of TE_{00} mode at 780 nm and 1560 nm, as shown in Figs. 1(b) and 1(c), respectively. We can see that the waveguide is designed to be single mode for the SPDC photons. Note that although here we considere the X-cut LN film, our method is also applied to the Z-cut LN film. The difference is that the extraordinary light modes required in type-0 SPDC correspond to the TE and TM modes for X-cut and Z-cut LN films, respectively.

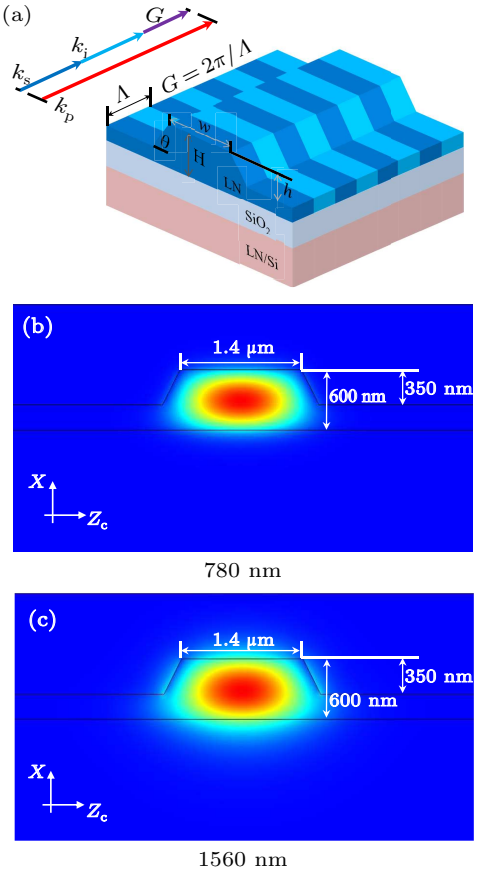

Fig. 1. (a) Schematic of PPLNOI waveguide structure and phase matching condition. Field distribution of the TE_{00} mode at the wavelength of 780 nm (b) and 1560 nm (c).

Considering the pump coupling to be optimized to excite the fundamental mode in the waveguide, and using a continues-wave (cw) laser light with a single frequency ω_p as the pump, we can write the two-photon term of SPDC as[28–30]

$$|\Psi\rangle = A \int \mathrm{d}\nu f(L\Delta k)\hat{a}_s^{\dagger}(\omega_{s0}+\nu)\hat{a}_i^{\dagger}(\omega_{i0}-\nu)|0\rangle, \quad (1)$$

where ν is frequency detuning from the signal and idler central frequencies ω_{s0} and ω_{i0} ($\omega_{s0} = \omega_{i0} = \omega_p/2$). The coefficient A absorbs all the constants and slowly varying functions of frequency, given by $A = \mathrm{i}\sqrt{2/\pi^3}(n_{g0}d_{33}LE_p\omega_p/3cn_0^2)$,[25] where c, d_{33}, E_p, n_{g0} and n_0 are the light velocity in vacuum, effective nonlinear coefficient, pump amplitude, the group refractive index and the refractive index of light at frequency $\omega_p/2$, respectively. The joint spectral amplitude function $f(L\Delta k)$ is determined by the phase-matching function, written as

$$f(L\Delta k) \propto \frac{1}{L}\int_0^L \mathrm{e}^{\mathrm{i}\Delta kz}\mathrm{d}z, \quad (2)$$

where z is the propagation direction, and Δk is the phase mismatch expressed as

$$\Delta k = k_p - k_s - k_i - G, \quad (3)$$

with k_p, k_s, and k_i representing the wave vectors of the pump, signal, and idler fields, respectively. The reciprocal wave vector $G = 2\pi/\Lambda$ results from periodic poling and here the period is designed to make the perfect QPM condition of $\Delta k = 0$ be satisfied at the central frequencies, namely, in the case of $\nu = 0$. Note that here a normalization factor of $1/L$ is introduced for normalization by the amplitude when $\Delta k = 0$, and in our simulation the length is fixed to $L = 6$ mm. For the case of single-frequency pump, the joint spectral intensity can be obtained by tracing the frequency of either photon, given by

$$P(\lambda) = |f(L\Delta k)|^2, \quad (4)$$

and the function relation of Δk and wavelength λ is expressed as

$$\Delta k = \frac{2\pi n(\lambda_p)}{\lambda_p} - \frac{2\pi n(\lambda)}{\lambda} - \frac{2\pi n(\lambda')}{\lambda'} - G, \quad (5)$$

where $\lambda'^{-1} = \lambda_p^{-1} - \lambda^{-1}$, and n is the effective refractive index. Note that all the wavelengths in this paper denote the vacuum wavelengths.

For a homogenous waveguide, phase mismatch Δk does not change along the z direction of the waveguide, and consequently, the joint spectral amplitude function given by Eq. (2) can be calculated as

$$f(L\Delta k) \propto \mathrm{sinc}\left(\frac{L\Delta k}{2}\right)\exp\left(-\mathrm{i}\frac{L\Delta k}{2}\right), \quad (6)$$

and the joint spectral intensity is then given by

$$P(\lambda) \propto \mathrm{sinc}^2\left(\frac{L\Delta k}{2}\right). \quad (7)$$

According to Maxwell's equations, the field nature of a waveguide is determined by its boundary conditions relating to the waveguide dimensions, such as thickness and width. For the strong-confined waveguide, a slight variation in dimension could have a great effect on the optical properties, like the refractive index, inducing the change of the phase-matching function. Here we focus on the effect of the thickness variation, denoted by $\Delta H(z)$, which would be a function of z for

an inhomogeneous variation. As a result, phase mismatch Δk becomes

$$\Delta k(z) = \Delta k_0 + \delta k(z), \tag{8}$$

where Δk_0 represents the phase mismatch when $\Delta H(z) = 0$, namely, $H = 600$ nm, and $\delta k(z)$ is the change of phase mismatch. In this case, the integration in Eq. (2) may be resolved as[31]

$$f(L\Delta k) \propto \frac{1}{L}\int_0^L \mathrm{e}^{\mathrm{i}\int_0^z \Delta k(\xi)\,\mathrm{d}\xi}\,\mathrm{d}z = \frac{1}{L}\int_0^L \mathrm{e}^{\mathrm{i}\Delta k_0 z}\mathrm{e}^{\mathrm{i}\int_0^z \delta k(\xi)\,\mathrm{d}\xi}\,\mathrm{d}z. \tag{9}$$

We simulate the values of δk for signal/idler wavelength ranging from 1200 nm to 1700 nm when $\Delta H = \pm 20$ nm, with the result shown in Fig. 2. We can see that δk can be considered to be independent of the wavelength. When the thickness change range is small, we can consider δk to be a linear function of the thickness increment ΔH, namely, $\delta k = a_0 \Delta H$,[32] and we can estimate $a_0 = -1.64 \times 10^{12}$ m^{-2} from the simulation result. Therefore, Eq. (9) is rewritten as

$$f(L\Delta k) \propto \frac{1}{L}\int_0^L \mathrm{e}^{\mathrm{i}\Delta k_0 z}\mathrm{e}^{\mathrm{i}a_0\int_0^z \Delta H(\xi)\,\mathrm{d}\xi}\,\mathrm{d}z. \tag{10}$$

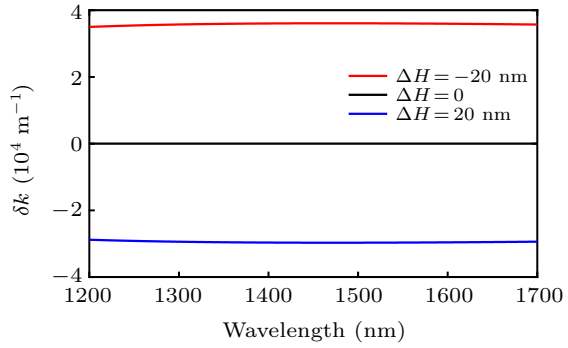

Fig. 2. Change of phase mismatch δk against wavelength under different thickness, with the thickness variation ΔH deviated from the designed thickness of 600 nm shown in the box.

3. Results

With numerical simulations via the COMSOL software, we can get the effective refractive index for different wavelengths, and then according to Eqs. (10) and (4), we can calculate the joint spectral amplitude function and the joint spectral intensity under any form of thickness variations, respectively.

We first simulate the joint spectral intensity in the case of the ideal designed structure when $\Delta H(z) = 0$, namely, $H = 600$ nm, which is given by Eq. (7). The simulation result is plotted in Fig. 3, which shows a sinc-square-type curve and the full width at half maximum (FWHM) can be estimated to be 159 nm.

Then we consider the linear deviation case, i.e., ΔH is a linear function of z, expressed as

$$\Delta H(z) = \kappa z + \sigma, \tag{11}$$

where κ and σ are two parameters determining the range of ΔH. Then the joint spectral intensity can be calculated as

$$P_2(\lambda) \propto \left|\frac{1}{L}\int_0^L \exp\left\{\mathrm{i}\left[(\Delta k_0 + a_0\sigma)z + \frac{1}{2}a_0\kappa z^2\right]\right\}\mathrm{d}z\right|^2. \tag{12}$$

A specific case is $\kappa = 0$ and $\Delta H = \sigma$, which is the homogenous case, i.e., ΔH does not change along the waveguide. Thus, we can obtain the joint spectral intensity as

$$P_3(\lambda) \propto \mathrm{sinc}^2\left[\frac{L(\Delta k_0 + a_0\sigma)}{2}\right]. \tag{13}$$

In Fig. 4, we show the simulation results of joint spectral intensities for $\Delta H = \pm 0.4$ nm, ± 0.8 nm, ± 1.2 nm, and ± 1.6 nm.

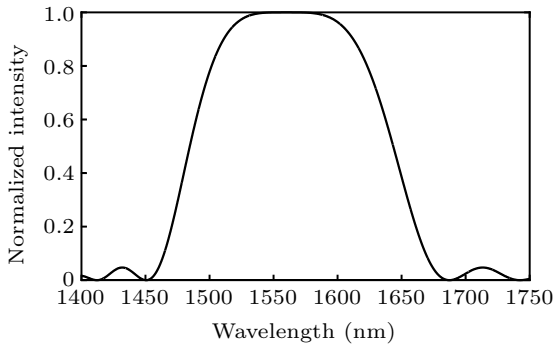

Fig. 3. Joint spectral intensity of the SPDC in the designed structure.

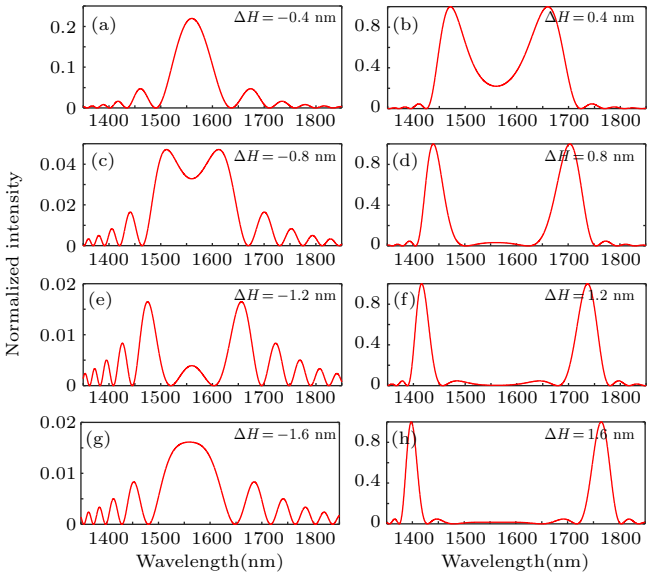

Fig. 4. Joint spectral intensity of the SPDC in the PPLNOI waveguides under different homogenous thickness variations ΔH, with the corresponding values of ΔH shown on the top right corner.

For $\kappa \neq 0$, this model corresponds to a linear variation of thickness ranging from $\sigma - \kappa$ to $\sigma + \kappa$ when z changes from 0 to L. In Fig. 5, we present some typical simulated results of the joint spectral intensities for several values of κ and σ.

By comparing the simulation results shown in Figs. 4 and 5 with the ideal joint spectral intensity plotted in Fig. 3, we can see that the thickness variation in several nanometers may have a distinct effect on the joint spectral intensity, such as narrowing or broadening the main peak, shifting the main

peak and splitting to multi-peaks. The original peak lies at 1560 nm, namely, the designed wavelength satisfying the perfect QPM condition of $\Delta k = 0$. The multi-peaks mean that, due to the thickness variations, some non-degenerate phase-matching amplitudes become bigger and may surpass the degenerate term. In particular, two prominent nondegenerate peaks occur in Figs. 4(d), 4(f), 4(h), and 5(k). In addition, from Fig. 5(g)–5(i), we can find that when $\Delta H = 0$ lies at $z = L/2$ the joint spectral intensity is not affected much by the thickness deviation, and the main peak is still at 1560 nm with a much broader bandwidth. For instance, as shown in Fig. 5(i), the bandwidth can be estimated to be 293 nm, which is nearly twice the value of the original bandwidth.

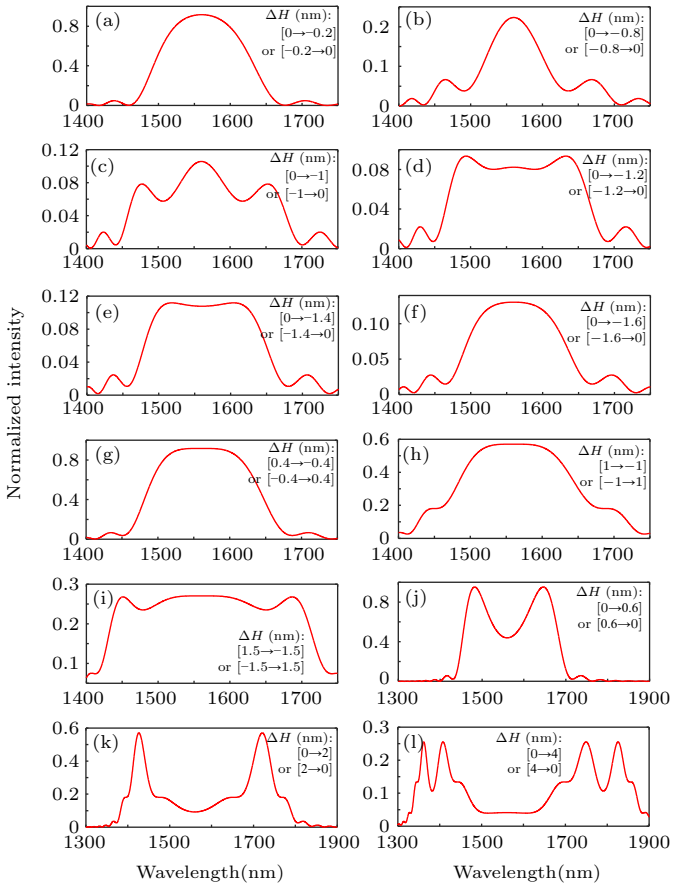

Fig. 5. Joint spectral intensity of the SPDC in the PPLNOI waveguides under the linear thickness variation ΔH along the waveguide, with the value ranges when z changes from 0 to L shown on the top right corner.

In fact, the surface of LNOI has certain irregular undulations, namely, roughness, and the root mean square (RMS) of the roughness is usually less than 1 nm.[2,8] In the entire wafer range, LNOI also has random fluctuations on thickness. For example, the commercial LNOI film from NANOLN Inc. has a thickness variation around 35 nm in a large range on a whole wafer.[33] To analyze the fluctuation noise on thickness, we introduce a noise parameter $\tau(z)$ and rewrite Eq. (11) as

$$\Delta H(z) = \kappa z + \sigma + \tau(z). \tag{14}$$

For the white noise, $\tau(z)$ fluctuates randomly around its average $\bar{\tau}$, and therefore, the integration in Eq. (10) can be calculated as $\int_0^z \tau(\xi)\mathrm{d}\xi = \bar{\tau}$. Hence in this case the noise model is equivalent to $\Delta H(z) = \kappa z + \sigma'$, with $\sigma' = \sigma + \bar{\tau}$.

The $1/f$ noise is another type of noise spectrum regarding to long-range fluctuations, which is characterized by spatial correlations.[27] We model the $1/f$ noise following the method in Ref. [27], and simulate the resulted joint spectral intensity. We find that the $1/f$ noise can bring a distinct effect to the joint spectral intensity. We present several typical results in Fig. 6, including the effects of narrowing, broadening, and splitting the central peak.

The above analysis is based on the numerical simulations of Δk. To further explain the effect in physical mechanism, we expand the signal and idler wave vectors around the central frequencies up to the second order in the detuning ν, respectively,

$$k_\mathrm{s}(\omega_{\mathrm{s}0}+\nu) = \frac{n(\omega_{\mathrm{s}0}+\nu)}{c} \approx \frac{n_0\omega_\mathrm{p}}{2c} + \frac{1}{u_0}\nu + \frac{g_0}{2}\nu^2, \tag{15}$$

$$k_\mathrm{i}(\omega_{\mathrm{i}0}-\nu) = \frac{n(\omega_{\mathrm{i}0}-\nu)}{c} \approx \frac{n_0\omega_\mathrm{p}}{2c} - \frac{1}{u_0}\nu + \frac{g_0}{2}\nu^2, \tag{16}$$

where u_0 and g_0 are the group velocity and group velocity dispersion (GVD) of light at the central frequency $\omega_{\mathrm{s}0} = \omega_{\mathrm{i}0} = \omega_\mathrm{p}/2$, expressed as

$$u_0 = \left.\frac{\mathrm{d}\omega}{\mathrm{d}k}\right|_{\omega=\omega_\mathrm{p}/2}, \tag{17}$$

$$g_0 = \left.\frac{\mathrm{d}^2k}{\mathrm{d}\omega^2}\right|_{\omega=\omega_\mathrm{p}/2}. \tag{18}$$

Then the phase mismatch given by Eq. (3) can be written as

$$\Delta k \approx -g_0\nu^2. \tag{19}$$

In this context, with a thickness increment $\Delta H(z)$, Eq. (8) becomes

$$\Delta k(z) \approx -g_0\nu^2 + a_0\Delta H(z). \tag{20}$$

With numerical simulation, we can obtain the GVD value as $g_0 = -80\times10^{-30}$ s^2/mm. Note that if substituting the value into Eq. (7), we would get a slightly broader bandwidth than 159 nm shown in Fig. 3, as this value only considers the dispersion up to the second order. However, such approximation is adequate to explain the effect on the spectrum.

It is well known that an efficient nonlinear process occurs when phase matching condition $\Delta k = 0$ is satisfied. In our design the phase matching frequency position is at $\nu = 0$, while due to the thickness variation the phase mismatch becomes $\Delta k(z) = a_0\Delta H(z)$. Thus, for the homogenous case given in Eq. (13), we can calculate that thickness deviations of $\Delta H = \pm0.11$ nm and ±0.16 nm would induce reducing factors of 0.9 and 0.8 to the amplitude at $\nu = 0$, respectively. We can

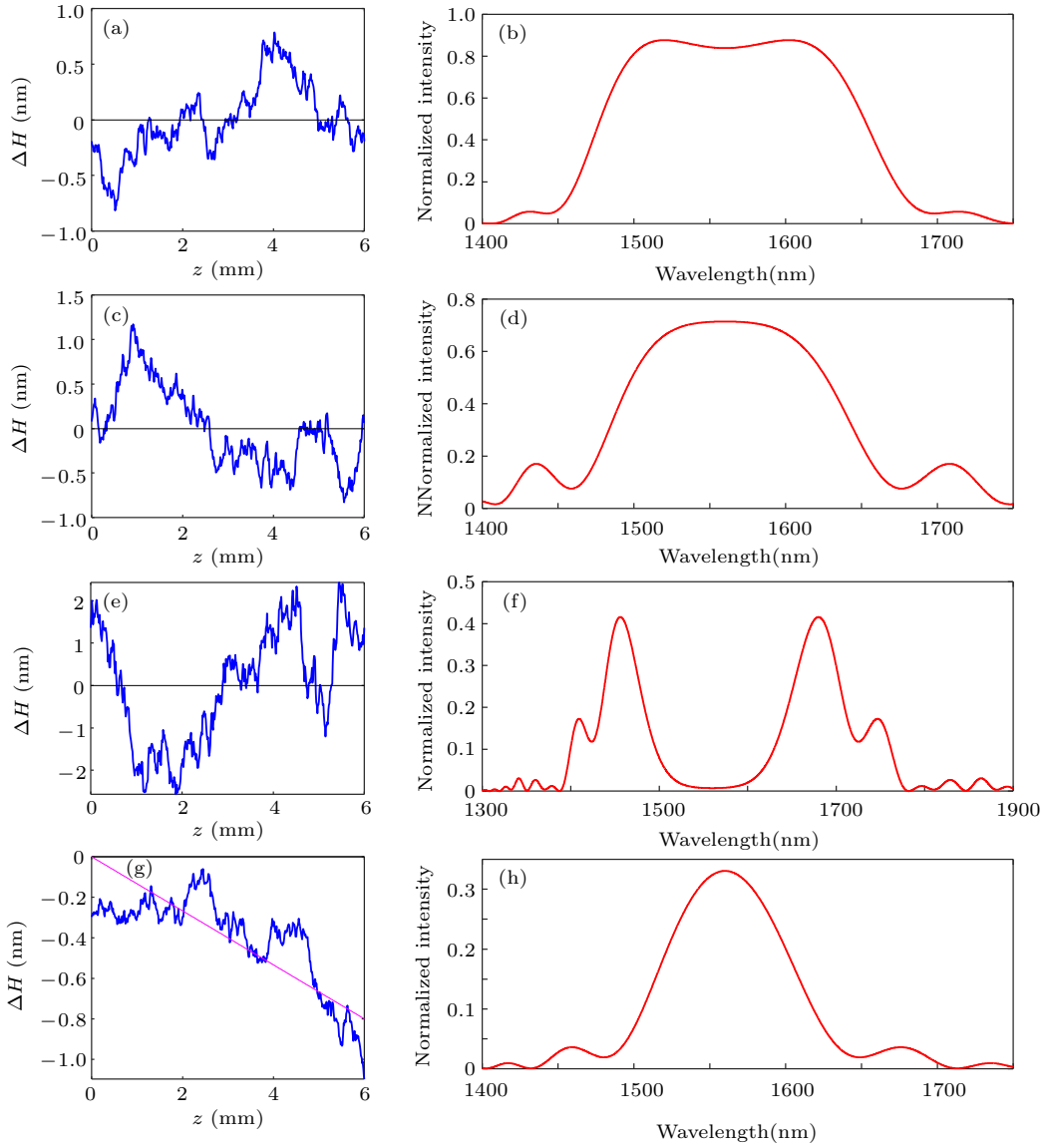

Fig. 6. Joint spectral intensity of the SPDC in the PPLNOI waveguides under thickness variations of $1/f$ noise model. The ranges of $1/f$ noise fluctuations shown in (a), (c), (e), and (g) are ± 0.8 nm, 0.2 ± 1 nm, ± 2.5 nm, and 0 to -1.4 nm, respectively.

also find that when $\Delta H > 0$ phase matching condition can be satisfied at $\nu = \pm\sqrt{a_0 \Delta H / g_0}$, and hence two prominent peaks appear at two nondegenerate positions as shown in Figs. 4(b), 4(d), 4(f), and 4(h). On the other hand, when $\Delta H < 0$ there is no phase matching frequency position, and therefore, as shown in Fig. 4(a), 4(c), 4(e), and 4(g), the whole amplitude is reduced despite the appearance of inefficient peaks. For the inhomogeneous variations, the phase matching frequency position changes with different z, and hence the total effect is a collective integration on z as shown in Eq. (10), and would be decreased compared with the homogenous case, as shown in Figs. 5 and 6.

4. Conclusion

We presented a detailed study on the effect of waveguide thickness variations on the frequency spectrum of photon pairs generated from SPDC in the PPLNOI waveguide. We first gave a general analysis on the effect and then numerically simulated the effect of several thickness variation models, including homogenous error, linear variation, white noise, and $1/f$ noise. We found that, due to the strong optical confinement in the LNOI waveguide, variations in several nanometers can have distinct effects on the joint spectral intensity. The central peak of the joint spectral intensity curve in the designed ideal case may be narrowed, broadened, and split to multi-peaks or two prominent peaks. We also found that the effects of positive and negative variations could be canceled, resulting in a variation-robust feature and a much broad bandwidth. Our study may be beneficial for the design of integrated photon sources in the LNOI platform and promote the development of LNOI-based photonic integrated technologies. Our analysis could provide a method for manipulating SPDC frequency states as well.

References

[1] Boes A, Corcoran B, Chang L, Bowers J and Mitchell A 2018 *Laser Photon. Rev.* **12** 1700256

[2] Jia Y, Wang L and Chen F 2021 *Appl. Phys. Rev.* **8** 011307

[3] Lin J, Bo F, Cheng Y and Xu J 2020 *Photon. Res.* **8** 1910

[4] Wang J, Sciarrino F, Laing A and Thompson M G 2020 *Nat. Photon.* **14** 273

[5] Weis R S and Gaylord T K 1985 *Appl. Phys. A.* **37** 191

[6] Krasnokutska I, Tambasco J J, Li X and Peruzzo A 2018 *Opt. Express* **26** 897

[7] Zhang M, Wang C, Cheng R, Shams-Ansari A and ončar M 2017 *Optica* **4** 1536

[8] Wu R, Wang M, Xu J, Qi J, Chu W, Fang Z, Zhang J, Zhou J, Qiao L, Chai Z, Lin J and Cheng Y 2018 *Nanomaterials* **8** 910

[9] Zhou J X, Gao R H, Lin J, Wang M, Chu W, Li W B, Yin D F, Deng L, Fang Z W, Zhang J H, Wu R B and Cheng Y 2020 *Chin. Phys. Lett.* **37** 084201

[10] Lin J, Xu Y, Fang Z, Wang M, Song J, Wang N, Qiao L, Fang W and Cheng Y 2015 *Sci. Rep.* **5** 8072

[11] Wang C, Langrock C, Marandi A, Jankowski M, Zhang M, Desiatov B, Fejer M M and Lončar M 2018 *Nature* **562** 101

[12] He M, Xu M, Ren Y, Jian J, Ruan Z, Xu Y, Gao S, Sun S, Wen X, Zhou L, Liu L, Guo C, Chen H, Yu S, Liu L and Cai X 2019 *Nat. Photon.* **13** 359

[13] Zhang M, Buscaino B, Wang C, Shams-Ansari A, Reimer C, Zhu R, Kahn J and Lončar M 2019 *Nature* **568** 373

[14] Wang C, Zhang M, Zhu R, Hu H and Lončar M 2019 *Nat. Commun.* **10** 978

[15] Armstrong J A, Bloembergen N, Ducuing J and Pershan P S 1962 *Phys. Rev.* **127** 1918

[16] Xu P and Zhu S N 2012 *AIP Adv.* **2** 041401

[17] Wang J, Zhang C H, Liu J Y, Qian X R, Li J and Wang Q 2021 *Chin. Phys. B* **30** 070304

[18] Tanzilli S, De Riedmatten H, Tittel H, Zbinden H, Baldi P, De Micheli M, Ostrowsky D B and Gisin N 2001 *Electron. Lett.* **37** 26

[19] Jin H, Liu F M, Xu P, Xia J L, Zhong M L, Yuan Y, Zhou J W, Gong Y X, Wang W and Zhu S N 2014 *Phys. Rev. Lett.* **113** 103601

[20] Montaut N, Sansoni L, Meyer-Scott E, Ricken R, Quiring V, Herrmann H and Silberhorn C 2017 *Phys. Rev. Appl.* **8** 024021

[21] Sun C W, Wu S H, Duan J C, Zhou J W, Xia J L, Xu P, Xie Z, Gong Y X and Zhu S N 2019 *Opt. Lett.* **44** 5598

[22] Zhang Q Y, Xu P and and Zhu S N 2018 *Chin. Phys. B* **27** 054207

[23] Zhao J, Ma C, Rüsing M and Mookherjea S 2020 *Phys. Rev. Lett.* **124** 163603

[24] Ma Z, Chen J Y, Li Z, Tang C, Sua Y M, Fan H and Huang Y P 2020 *Phys. Rev. Lett.* **125** 263602

[25] Xue G T, Niu Y F, Liu X, Duan J C, Chen W, Pan Y, Jia K, Wang X, Liu H Y, Zhang Y, Xu P, Zhao G, Cai X, Gong Y X, Hu X, Xie Z and Zhu S N 2021 *Phys. Rev. Appl.* **15** 064059

[26] Santandrea M, Stefszky M and Silberhorn C 2019 *Opt. Lett.* **44** 5398

[27] Santandrea M, Stefszky M, Ansari V and Silberhorn C 2019 *New J. Phys.* **21** 033038

[28] Santandrea M, Stefszky M, Roeland G and Silberhorn C 2019 *New J. Phys.* **21** 123005

[29] Tian X H, Zhou W, Ren K Q, Zhang C, Liu X, Xue G T, Duan J C, Cai X, Hu X, Gong Y X, Xie Z and Zhu S N 2021 *Chin. Opt. Lett.* **19** 60015

[30] Gong Y X, Xie Z D, Xu P, Yu X Q, Xue P and Zhu S N 2011 *Phys. Rev. A* **84** 053825

[31] Helmfrid S, Arvidsson G and Webjörn J 1992 *J. Opt. Soc. Am. B* **10** 222

[32] Santandrea M, Stefszky M and Silberhorn C 2019 *Opt. Lett.* **44** 5398

[33] NANOLN Inc., private communication